Trimmed CFD Simulation of a Complete Helicopter Configuration

W. Khier*, M. Dietz, T. Schwarz* and S. Wagner****

*Institut für Aerodynamik und Strömungstechnik,
Deutsches Zentrum für Luft- und Raumfahrt e.V. (DLR)
Lilienthalplatz 7, 38108 Braunschweig, Germany
email: walid.khier@dlr.de

**Institut für Aerodynamik und Gasdynamik, Universität Stuttgart
Pfaffenwaldring 21, 70569 Stuttgart, Germany
email: dietz@iag.uni-stuttgart.de

Keywords: Weak coupling, elastic blades, pitch up, tail shake, aerodynamic interference, helicopter aerodynamics.

Abstract: An investigation was carried out using the flight mechanics tool HOST weakly coupled to the RANS solver FLOWer to simulate the flow around helicopter configuration under different flight conditions. The configuration considered was a wind tunnel model with powered 4.2 meter four-bladed main rotor, and 0.73 meter two bladed tail rotor. Two forward flight conditions at Mach number equal to 0.059 and 0.204 were considered at 5^o and -2^o angle of attack, respectively. The objective was to asses the aerodynamic interference between helicopter components by comparing the main rotor and fuselage loads with their counterparts obtained from isolated fuselage and isolated rotor simulation. The study revealed noticeable changes in the load distribution on the main rotor between the isolated rotor and full helicopter cases, but only negligible differences in power consumption resulted. Major changes in the fuselage loads and surface pressure were also found.

INTRODUCTION

Over the past few decades, an ever-growing trend towards the application of computational fluid dynamics (CFD) in helicopter aerodynamics has evolved. Owing to the complexity of the flow around helicopters, and also lack of computational resources, early simulation approaches could only utilize simplified, linear physics ([1] and [2]). The evolution of modern powerful computers enabled the application of Euler, and later Reynolds-Averaged Navier-Stokes (RANS) solvers in helicopter aerodynamics. However, due to the severity of the problem, most of the recent numerical simulation efforts have been limited either to isolated rotors, as in [3]-[7], or isolated fuselages ([8]-[12]).

Accurate prediction of rotor aerodynamics requires adequate simulation of blade dynamics and elastic deformation. Rigid blade assumption yields a different onset of the flow along the blades than that encountered in reality, and thus degrades the quality of computations ([3], [5] and also [14]). The aerodynamics of the isolated fuselage is characterized by complex, essentially three-dimensional flow field with large regions of flow separation, which require high resolution in space, and sometimes in time when the flow instabilities are too strong to be averaged by the solver. Simulation of a complete helicopter involves not only mutual influence of the fuselage and main rotor on their flow regimes, but additional flow phenomena caused by their interaction with other components of the helicopter as well.

The aerodynamic interference between helicopter components may seriously affect the performance, operation and safety of helicopters. Blade-vortex interaction, for example, increases the noise levels produced by the rotor. Uncomfortable vibrations to the pilots and passengers may take place under certain flight conditions owing to pulsating excitation by the wake of main rotor hub at, or close to, the natural frequency of the tail unit [13].

The effect of the rotating blades can be realized in CFD either by explicit resolution of the motion ([14]-[16]), using overlapping or sliding grids, or a re-meshing technique. Development of a periodic flow field around the helicopter is achieved after several rotor revolutions depending on how rapid the wakes of the fuselage and the rotor are transported downstream. Alternatively, an actuator disc may be employed, as in [17] and [18], to represent the effect of the rotor on the flow field. This is realized by imposing prescribed radial and azimuth distributions of mass flow and momentum jump calculated by a rotor simulation tool. Thus, reaction of the fuselage on the flow field can not be returned back to the fight mechanics module to update the trim the rotor or to deformation of the rotor disc geometry in a similar fashion to references [19]-[22].

In this paper time accurate RANS simulation of the flow past a complete helicopter configuration is reported. The study considered two forward flight conditions at low and medium speeds. Both the main rotor and the fuselage of the complete configuration were simulated separately under the same flight conditions. Whenever the rotor was considered, weak fluid-structure coupling was applied to generate predefined thrust and propulsive force, and to obtain the deformation of the blades. The coupling procedure will be only described briefly. A detailed description on the coupling process and its application to a complete helicopter configuration using multiblock blade grids is given in [20]. The three configurations were compared in terms of aerodynamic loads, surface pressure distribution and wake structure to analyze the aerodynamic interaction between the rotating and non-rotating components of the helicopter. A part of the computations represents some of the blind test activities of the EU project GOAHEAD [23]. An overview of the project and the blind test activities is given by [24] and [25], respectively.

APPROACH

Time accurate RANS computations were carried out using the DLR CFD method FLOWer [26]. FLOWer is based on a central scheme and finite volume discretization. Time accurate computations are performed as a series of steady state computations via dual time stepping. Each physical time step, a steady state solution is sought by marching in an artificial time via a multi-step Runge-Kutta method. In the presented computations, implicit residual smoothing and local time stepping, in addition to multigrid were applied to speed up the convergence. Turbulence effects were introduced by a slightly modified version [27] of Wilcox's two-equation k-ω model [28] as a compromise between accuracy robustness and computational costs. Blade motion was achieved using Chimera method [29].

The rotor was trimmed to pre-defined weight, lateral and propulsive force coefficients using the stand alone flight mechanics tool HOST (Helicopter Overall Simulation Tool) [30]. The resulting rotor controls and elastic deformation of the blade surface for the whole radial and azimuth range were then imposed on the CFD simulation to modify the blade surface geometry following the approach presented in [19]-[21]. The process was repeated until the variation in elastic blade deformation and rotor control angles have fallen below a user defined tolerance.

SIMULATED TEST CASES AND NUMERICAL GRID

Two flight conditions associated with pitch up and tail shake phenomena were considered. During pitch up, the main rotor wake impinges on the horizontal stabilizer giving rise to nose-up moments acting on the helicopter about its lateral axis. This phenomenon is frequently encountered during slow transition from hover to cruise. Tail shake is a wake induced vibration problem arising from interference between the wake of main rotor hub and the tail part. An analysis of the tail shake problem is beyond the scope of this study as it is a mixed problem involving structural analysis of the fuselage. In this paper only the aerodynamic phenomena associated with the tail shake will be investigated rather than the tail shake itself. In both cases the main rotor was trimmed to overcome a predefined aerodynamic drag and to generate vertical force equal to a nominal weight. Main rotor collective, longitudinal and lateral cyclic pitch components were set free in the trim process. Table 1 summarizes the flight conditions and trim objectives for both cases.

	Pitch up	Tail shake
Free stream Mach number Ma [.]	0.059	0.204
Fuselage attitude α [^{o}]	+5	-2
Main rotor tip Mach number M_{tip} [.]	0.617	
Tail rotor tip Mach number $M_{tip,\,tr}$ [.]	0.566	
Main rotor loading C_t/σ [.]	0.071	0.071
Main rotor lateral force coefficient C_y [.]	0	
Propulsive force coefficient C_xS [m^2]	-0.176	-0.185
Free parameters	$\theta_0,\theta_c,\theta_s$	

Table 1: Summary of the flight and trim parameters

Where C_t is the rotor vertical force coefficient, σ is the main rotor solidity, C_y is the main rotor lateral force coefficient, C_x is longitudinal force coefficient in the flow direction, S is a reference area, $\theta_0,\theta_c,\theta_s$ are the main rotor collective, longitudinal and lateral cyclic pitch angles, respectively.

The computational model refers to the GOAHEAD wind tunnel model [25]. It consists of a 4.1 m NH90 fuselage model, ONERA 7AD main rotor, reduced scale BO105 tail rotor, a simplified rotor hub, a strut and slip ring fairing and 8m x 6m test section of 20m length (Figure 1). Both the main and tail rotors are represented by isolated blades. The main rotor hub is simplified to a cylindrical element and an elliptical hub fairing.

Multi-block grids around the different elements were combined via Chimera to build three different computational configurations: an isolated rotor, an isolated fuselage and a complete helicopter. Figure 1 depicts the surface grid for the complete helicopter configuration, while Table 2 lists the characteristics of the numerical grid for the three configurations.

	No. of blocks	Number of points	Isolated rotor	Isolated fuselage	Complete helicopter
Fuselage	90	9 500 000		X	X
Main rotor blade (x 4)	10	870 000	X		X
Tail rotor blade (x 2)	3	350 000			X
Rotor hub	8	900 000		X	X
Strut	12	530 000		X	X
Wind tunnel (background 1)	13	300 000		X	X
Wind tunnel (background 2)	26	3 100 000	X		
Total (blocks/Million point)			66/6.5	123/11.2	169/15.4

Table 2: Grid parameters

No slip conditions were applied on all solid surfaces of the helicopter, and slip condition on tunnel walls. Flow variables at inflow and outflow boundary were derived from one-dimensional characteristic theory. Figure 2 contains a sketch of the computational domain and the applied boundary conditions.

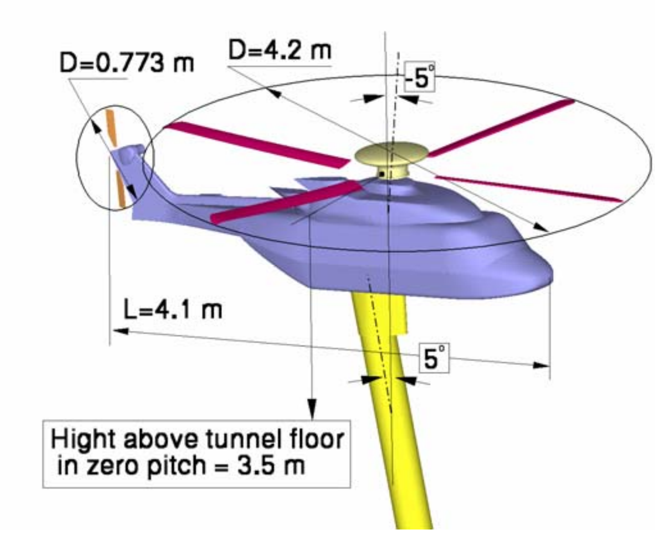

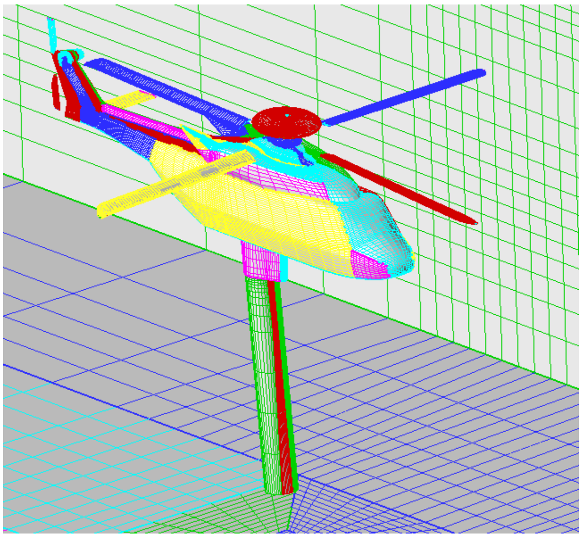

Figure 1: Left: Overview of the computational model showing its main components. Wind tunnel section not shown. Right: Surface grid on the model and wind tunnel walls

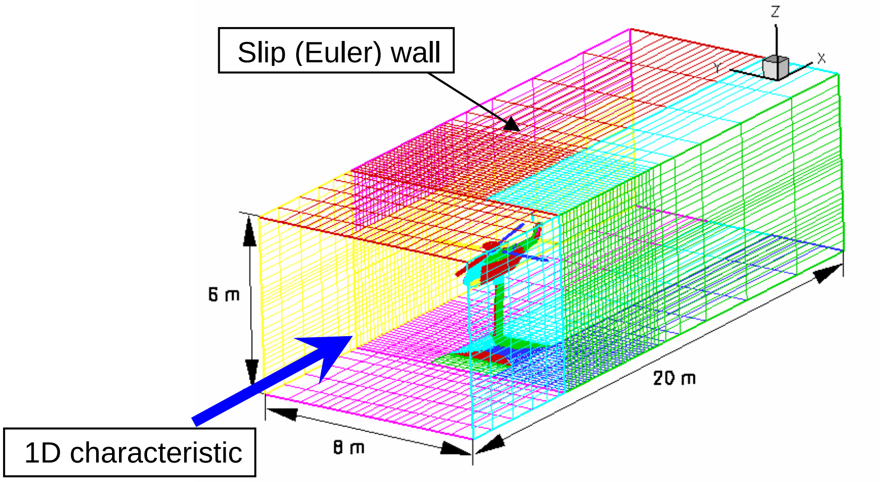

Figure 2: Overview of the computational domain showing the boundary conditions applied at tunnel's inlet, outlet and walls

RESULTS

Figure 3 and Figure 4 compare the computed pressure coefficients on the blade for the isolated rotor and the complete helicopter. In the tail shake case (Figure 3) the differences are most obvious on the suction in the advancing range up to $\Psi=60^o$, and on the pressure side for the $\Psi=90^o$ position. No significant differences can be observed for the rest of the azimuth range up to $\Psi=300^o$, where higher and lower pressure develop respectively on the pressure and suction sides indicating higher local lift for the complete helicopter case than in the isolated rotor case. The corresponding differences are more or less constant in the pitch up case. Slightly lower pressure on the suction side in the isolated rotor case than in the complete helicopter case is consistently observed.

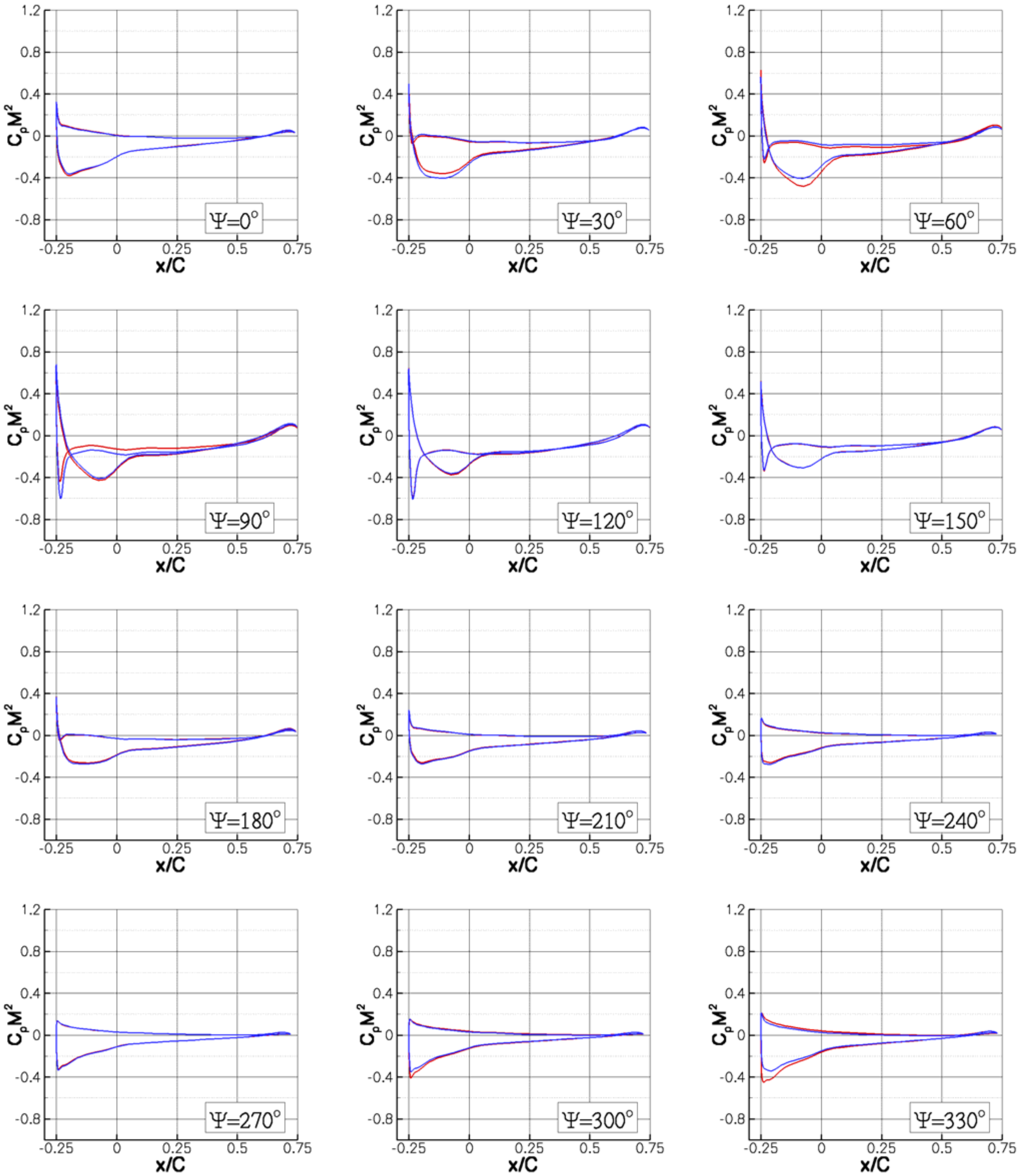

Figure 3: Computed pressure distribution on the blade vs. azimuth angle Ψ. Free stream mach number, Ma = 0.204, fuselage attitude, $\alpha = -2^{o}$, r/R=0.92. Red: complete helicopter. Blue: Isolated rotor.

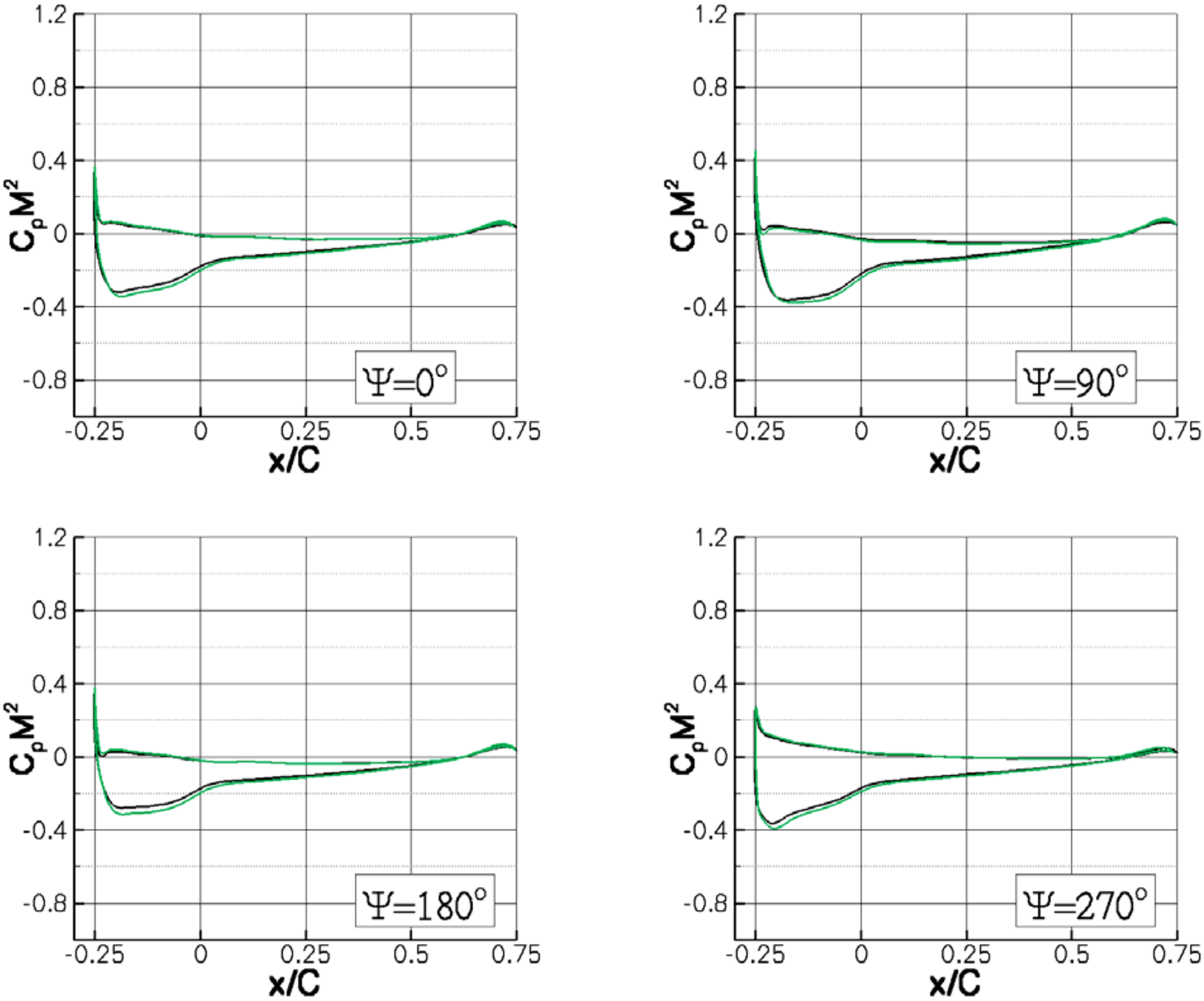

Figure 4: Computed pressure distribution on the blade vs. azimuth angle Ψ. Free stream Mach number, Ma = 0.059, fuselage attitude, α=5°, r/R=0.92. Black: complete helicopter. Green: Isolated rotor.

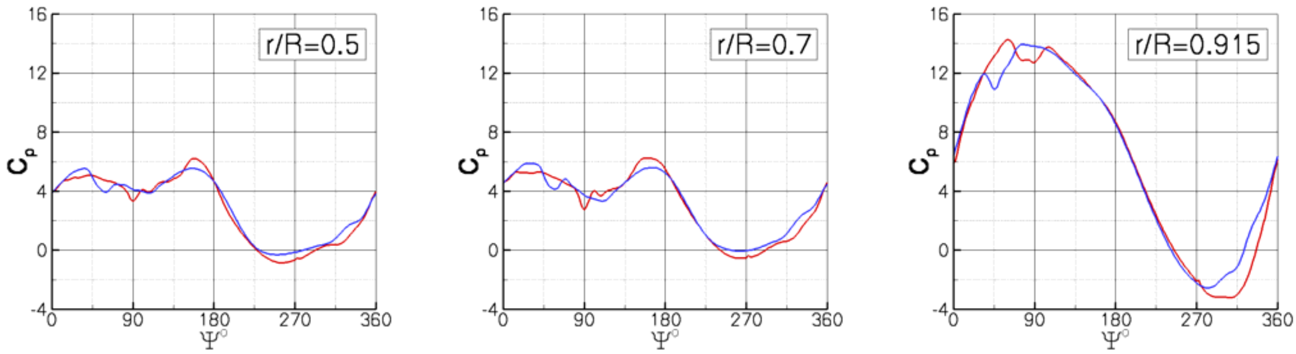

Figure 5: Computed pressure coefficient vs. azimuth angle Ψ on the leading edge of the blade at three radial positions. Free stream mach number, Ma = 0.204, fuselage attitude, α=–2°, Red: complete helicopter. Blue: Isolated rotor

Figure 5 shows the time history of the leading edge pressure coefficient at selected radial positions. Similar to the sectional pressure plots, minor differences can be seen except in the retreating range $\Psi=270^o-360^o$. Pressure oscillation can be observed between $\Psi=0^o$ and $\Psi=90^o$ for the isolated rotor case indicating torsional deformation in the inboard part of the blade.

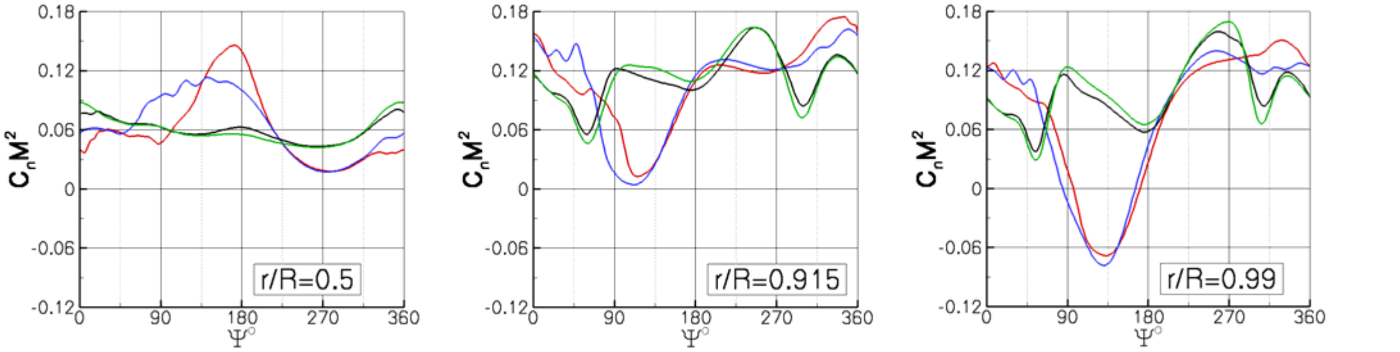

Figure 6: C_nM^2 as a function of the azimuth angle at selected radial positions for the complete helicopter (red) and the isolated rotor (blue) under tail shake flight conditions. The corresponding comparison for the pitch up case is represented by the black (complete helicopter) and green (isolated rotor) lines.

The evolution of the normal load distribution at three different radial positions is shown in Figure 6, and on the entire rotor disc in Figure 7. From the figures it can be clearly seen that the load distribution in tail shake is characterized by high load zones in the outboard region of the blade in the rear and front parts of the rotor disc (Figure 7.a and Figure 7.b). The tip region generates negative load in the second quarter between $\Psi=90^o$ and $\Psi=180^o$. Negative loading can also be found around the root of the retreating blade. The load intensity and location of extrema however

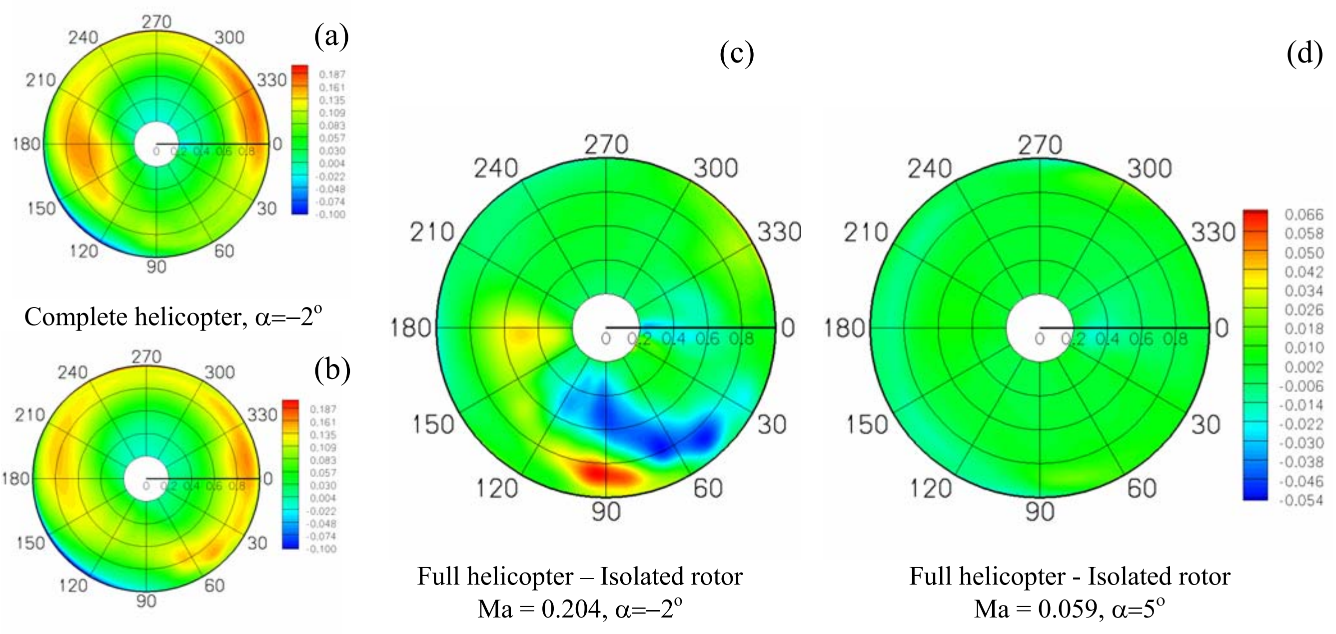

Isolated rotor, $\alpha=-2^o$

Figure 7: Right: C_nM^2 as a function of the azimuth angle for selected radial position for the complete helicopter (a) and the isolated fuselage (b): ΔC_nM^2 contours are shown for the tail shake (c) and pitch up cases (d).

depend on the configuration. This can be best deduced by plotting the deviation in load between the complete configuration and the isolated rotor over the rotor disc as shown in Figure 7.c. The interference with the fuselage can be traced in the figure close to $\Psi=180^o$ where an upward deflection of the flow over the windshield and engine fairing increases the effective angle of attack, and thus, causes an increase in normal loading around r/R=0.3. The load falls below that of the isolated rotor in the inboard region when the wake of the rotor hub encloses the blade, reaching its minimum as the blade passes over the tail boom ($\Psi=0^o$). Except for a slight increase near $\Psi=330^o$, the differences become nearly independent of the azimuth and radial location within the retreating range ($\Psi=180^o$-360^o). The discrepancy between the two rotors becomes too complex to explain in the advancing half as it involves elastic effects, trim and interactional phenomena. An analogous comparison for the pitch up case did not lead to a similar outcome (Figure 7.d) to that of the tail shake case. The low speed of flight generates wake with vortical structures of low intensity downstream of the non rotating parts. Hence, the wake-wake interference is reduced leaving flow blocking effects only, which do not seem to have a noticeable influence on the rotor aerodynamics except in the inboard region near $\Psi=0^o$ and close to the tip within the front part of the rotor disc.

Despite the importance of the observed differences with respect to flow physics, they have a minor impact on the average value of the main rotor loads as can be deduced from Figure 8. The aerodynamic coefficients presented in the figure are based on the rotor radius and disc area, and free stream conditions. Aerodynamic moments are estimated at the centre of the main rotor about an X-axis parallel to the flow, a Y-axis parallel to the lateral axis of the wind tunnel, and a Z-axis normal to the tunnel floor.

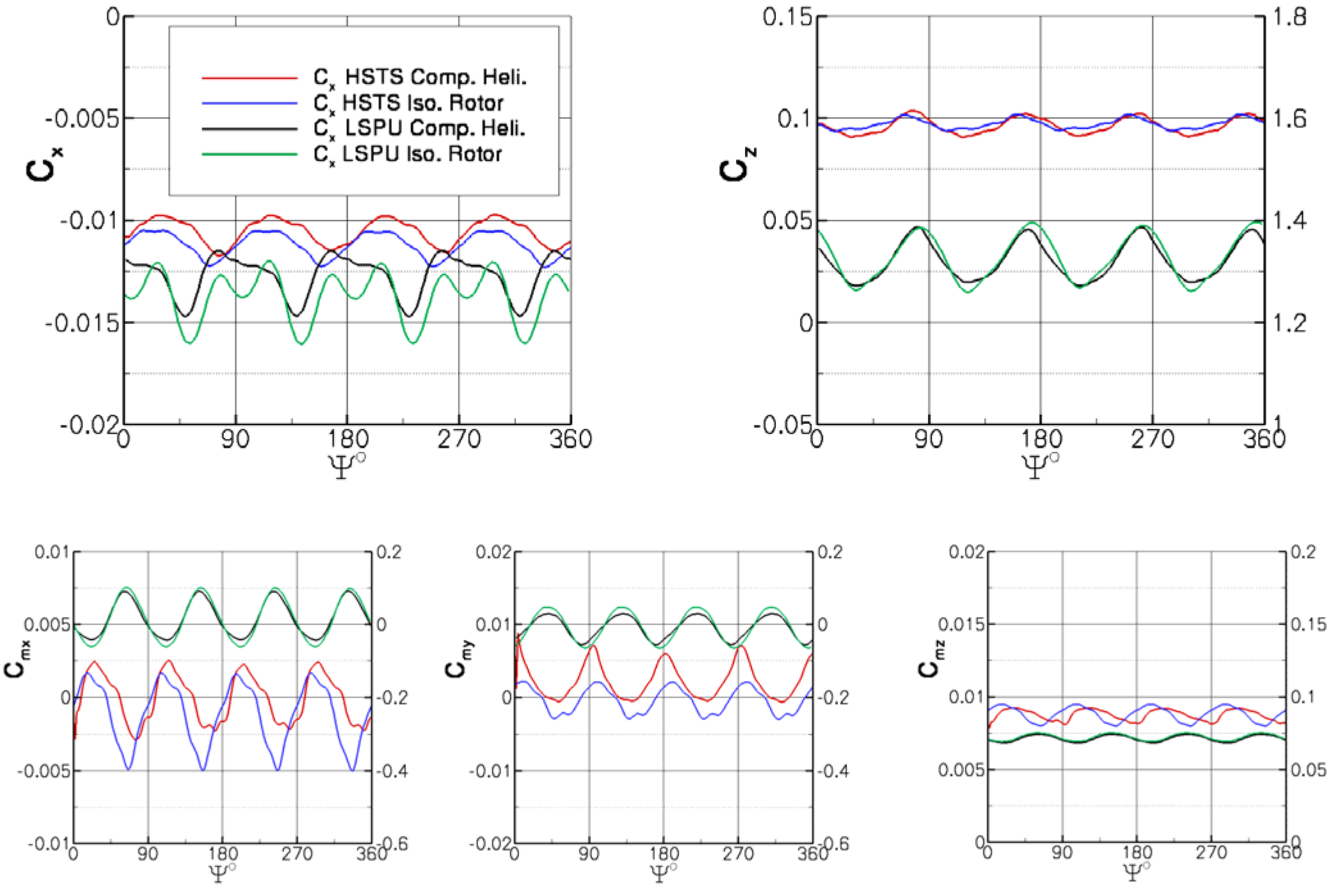

Figure 8: Comparison of computed rotor loads for the complete helicopter (red and black) and isolated rotor (blue and green). HSTS denotes tail shake and LSPU refers to pitch up. Whenever used the scale on the right corresponds to pitch up. Negative C_x values indicate propulsion, positive values refer to drag.

Since the same trim objectives were applied for both configurations, it is not surprising to find close agreement between isolated rotor and the complete helicopter results in terms of average values of propulsive and vertical forces. A 4/rev behaviour dominates the evolution of all coefficients superimposed with higher harmonics of negligible magnitude can be traced, except for the propulsive force in pitch up. In that particular case, higher (predominantly the eighth) harmonic contributions is observed with an amplitude nearly equal 20% of the peak to peak value. As for the amplitudes and phase, there is no clear reason why a similar agreement should be assumed. In fact discrepancy is what to expect since generation of the same forces in different flow fields results in different unsteady dynamic and elastic responses. One would also intuitively presume the deviation to depend on the flight speed to some extent as a result of a stronger interaction.

The variation of the moments with the azimuth angle is in line with the previous arguments. Slight, yet noticeable, lead and lag discrepancies are clearly visible in the tail shake case for the different moment components, whereas the pitch up results are pretty much in phase in comparison. The aerodynamic interaction seems to have a damping effect on the aerodynamic moment, except about the lateral axis (C_{my}) in tail shake. Furthermore, the trim of the rotor in tail shake results in an average roll moment (about the tunnel axis) equal to zero for the rotor of the complete configuration, and negative moment for the isolated rotor. Opposite trend is observed for the pitching moment where the rotor of the complete helicopter is subject to a slight nose up moment.

	Tail shake (Ma = 0.204, $\alpha=-2^o$)	Pitch up (Ma = 0.059, $\alpha=5^o$)
Complete helicopter	84.41 (kW)	51.08 (kW)
Isolated rotor	85.10 (kW)	51.84 (kW)

Table 3: Main rotor power consumption.

Examination of the computed main rotor power consumption listed in Table 3 reveals however a negligible increase of 0.69 kW for the tail shake, and a gain of 0.76 kW for the pitch up, as a result of including the non rotating elements in the simulation. This finding comes against expectation because it predicts a reduction in power consumption when interference between the rotor and the rest of the helicopter takes place. Since the rotors are trimmed to generate the same forces, the gain can be only attributed to a reduction in aerodynamic resistance. A thorough explanation is however difficult to make in view of the multitude of factors involved.

In Figure 9 the influence of the rotor on the fuselage is expressed by the deviation of averaged pressure obtained in the complete helicopter case from the isolated fuselage results. Pressure distribution on the isolated fuselage is also shown. The variation in pressure caused by aerodynamic interference clearly depends (in terms of pressure coefficient) on advance ratio. An asymmetrical pressure increase is seen in tail shake on the top of the cockpit and on the engine fairing. The presence of the tail rotor causes the pressure to decrease on the leading edge of the tail fin. Compared to the isolated fuselage, there is an evident increase of pressure coefficient of about 0.3 on the upper (pressure) side of the horizontal stabilizer. Owing to the low flight speed in pitch up the rotational symmetry of the flow around the rotor is not strongly distorted. This is expressed by a more or less uniform pressure increase in the windshield and engine fairing, and a nearly symmetric increase on the tail boom. Unlike the tail shake case, the main rotor intensifies the pressure on the tail fin's leading edge. Development of pitch up can be traced by an acute increase in pressure on the horizontal stabilizer. As far as the isolated fuselage cases are concerned, only the effects of different angles of attack can be observed.

Figure 10 presents a quantitative confirmation to the previous analysis in terms of pressure coefficient plots in the symmetry plane of the fuselage. In tail shake, the rotor wake increases the pressure on the upper side of the engine fairing between X=1 and X=1.5, and causes a lateral

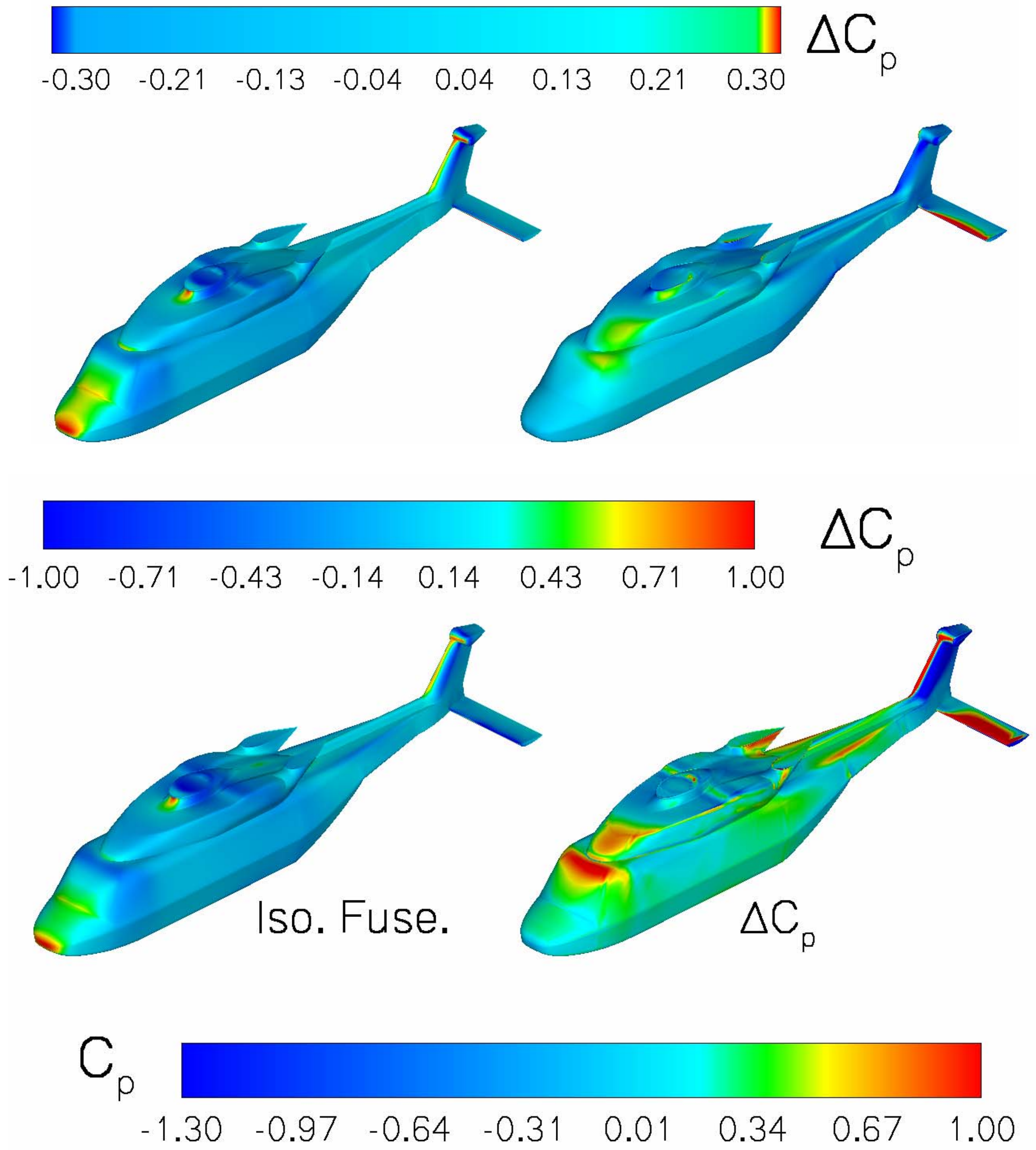

Figure 9: Surface pressure contours. Left: steady solution (isolated fuselage). Right: difference between averaged unsteady pressure (complete helicopter) and isolated fuselage pressure. Note the differences in scale. Top: Tail shake, Ma = 0.204, fuselage attitude, $\alpha=-2^{o}$. Below: Pitch up, Ma = 0.059, fuselage attitude, $\alpha=5^{o}$.

acceleration of the flow over the fairing of the tail rotor propeller shaft (on the top of the tail boom) causing the pressure to drop slightly there. In pitch up, the wake of the main rotor encloses the fuselage owing to the low speed of flight thus leading to a considerable increase in pressure on the upper side. On the lower side, negligible differences are observed under tail shake conditions, whereas a clear increase in pressure is detected in pitch up. This observation, which may seem confusing at first glance, can be explained by examining the pressure distribution across the wind

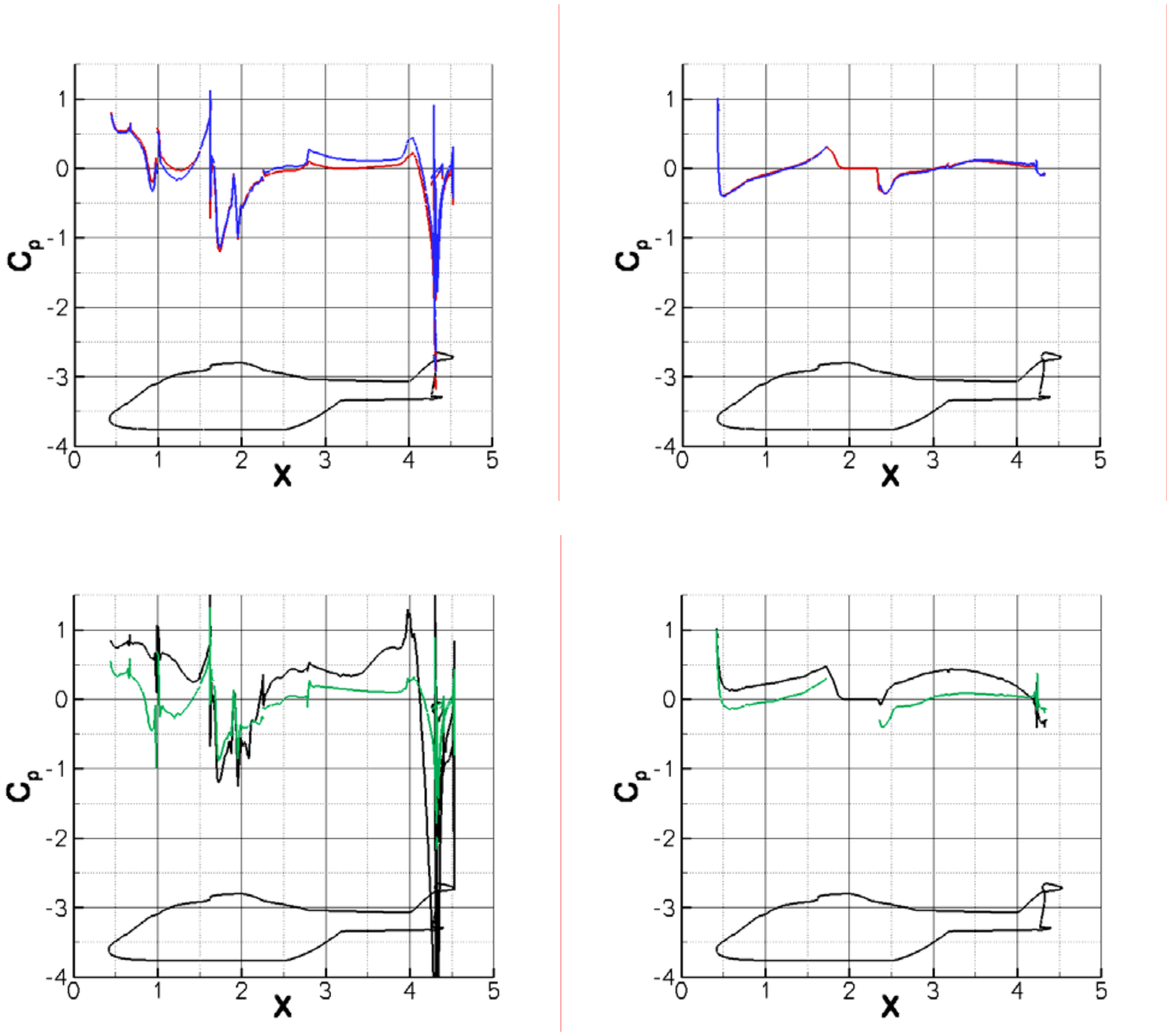

Figure 10: Top: Comparison of computed pressure at symmetry plane of the fuselage in tail shake for the full helicopter and isolated fuselage in red and blue respectively on the upper side (left), and on the lower side (right). Below: The corresponding results for pitch up in black and green. The range between X=1.85 and X=2.4 on the lower side is covered by the strut fairing.

tunnel presented in Figure 11. From the figure it can be clearly seen that the floor and walls have a non trivial effect, at least qualitatively, on the resulting pressure inside the tunnel in the complete helicopter case. This is mainly because the tunnel walls block the vertical and cross components of the momentum added by the rotor. When the advective transport of the incoming flow is not strong enough to convert these components to the direction of the incoming flow, the advective contents vanish at the walls giving rise to static pressure across the tunnel. Thus the process depends predominantly on the strength of advective mixing of the incoming flow and the added momentum by the rotor, or in other words, depends on the velocity of the flow and the generated thrust by the rotor, as indicated in the figure.

Figure 12 and Figure 13 support the previous qualitative analysis given in Figure 9 and Figure 10 by pressure sensor data at selected locations on the fuselage for tail shake and pitch up, respectively. In addition to the unsteady signal, the figures compare the mean pressure obtained in the complete helicopter cases with the isolated fuselage data. On the upper side, a 4/rev pulsation is evident in both cases. Pressure peaks are shifted around $\Psi=90^{o}$ and its multiples depending on the

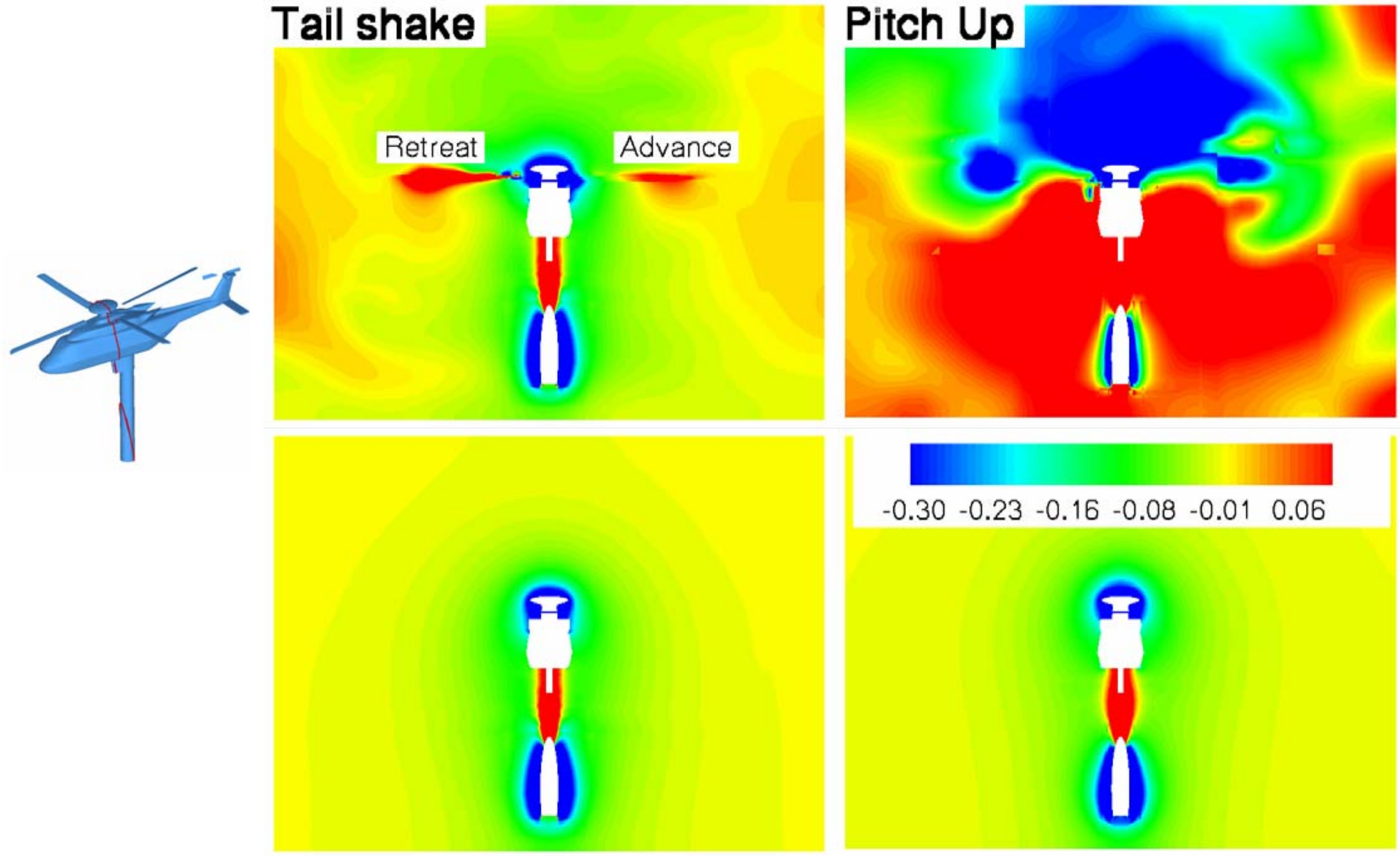

Figure 11: Pressure coefficient distribution across the tunnel in a plane formed by the main rotor axis and the lateral axis of the tunnel. The section contains the main rotor centre. Note the relative inclination between the rotor axis and strut results in irregular cut through the slip ring and strut fairing. Top row: complete helicopter. Below: isolated fuselage results. Tail shake pressure is shown on the left, pitch up on the right.

location of the sensor. A 10/rev behaviour can be clearly seen on the tail fin, except on the leading edge in tail shake (Figure 12.f). For this particular case the situation is less clear since several factors contribute to the evolution of pressure, possibly including the wake of the fuselage, the main rotor and the rotor hub.

The impact of the main rotor on the fuselage surface pressure is most clearly found on the front end of the helicopter in both cases where a significant increase in pressure coefficient is noticed. The influence of the advance ratio on the aerodynamic interference can be deduced by comparing the pressure evolution on the windshield presented in Figure 12.b and Figure 13.b. The high velocity of the flow undermines the pressure build up on the retreating side retaining the average pressure value nearly equal to the isolated fuselage case. The effect is much weaker in pitch up where the pressure on both the retreating and advancing sides is significantly higher than in the isolated fuselage. The rotor downwash alters the effective angle of attack on the horizontal stabilizer creating a high pressure zone on the upper side (see Figure 14). Consequently, strong acceleration of the flow takes place over the leading edge of the horizontal stabilizer associated by sharp suction peaks as indicated in Figure 13.f. The figure also reveals considerable discrepancy in pressure along the span. This is mainly caused by the short span of the stabilizer which increases the pressure rapidly as the ends are approached due to three-dimensional effects as shown in Figure 15.

The forces acting on the fuselage of the complete helicopter are compared to the isolated fuselage forces in Figure 16 for the tail shake case. Free stream conditions, unit length and unit area were

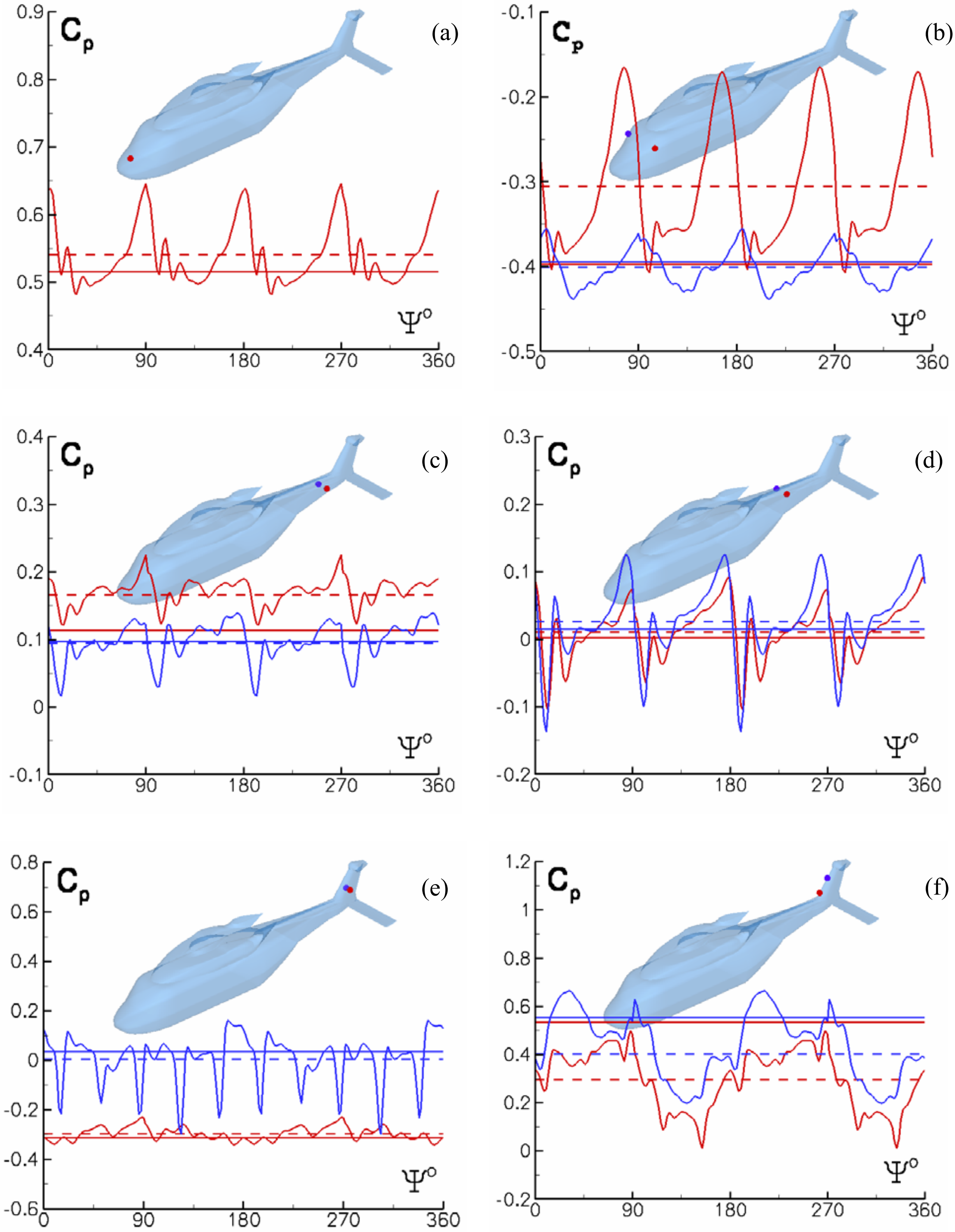

Figure 12: Comparison of instantaneous pressure signal (complete helicopter) and steady pressure (isolated fuselage). Curves denote unsteady pressure signals, dashed lines denote arithmetic average and straight lines refer to steady pressure. Free stream mach number, Ma = 0.204, fuselage attitude, $\alpha = 2^{o}$.

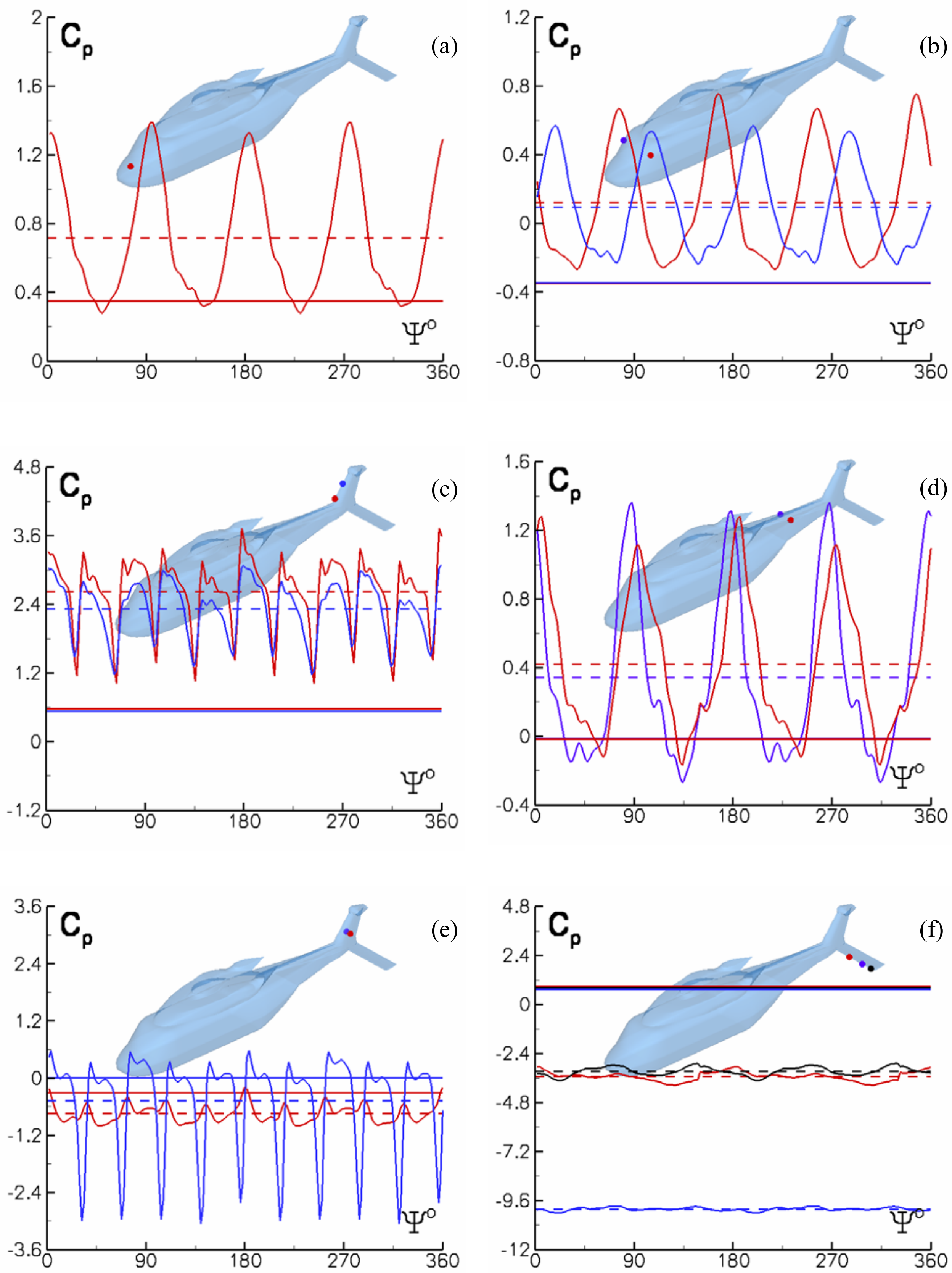

Figure 13: Comparison of instantaneous pressure signal (complete helicopter) and steady pressure (isolated fuselage) in pitch up. Curves denote unsteady pressure signals, dashed lines denote arithmetic average and straight lines refer to steady pressure. Free stream mach number, Ma = 0.059, fuselage attitude, $\alpha=5^o$.

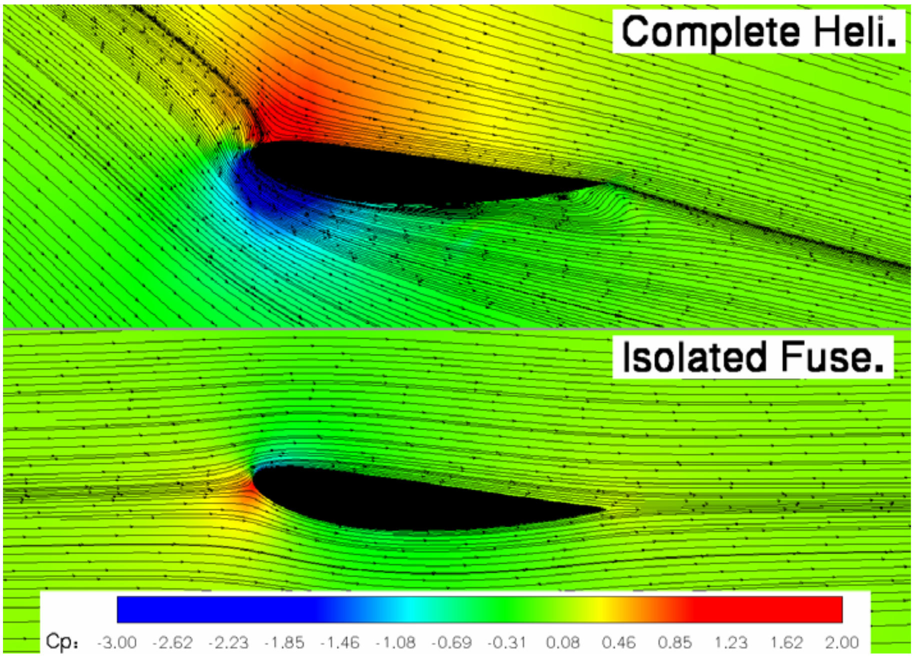

Figure 14: A cross section of the flow field at Y=0.5 m showing the effect of main rotor downwash on the flow structure in the vicinity of the stabilizer in pitch up. Free stream mach number, Ma = 0.059, fuselage attitude, $\alpha=5^{o}$

used to compute the aerodynamic coefficients. The changes in force coefficients remain below 0.05. Aerodynamic interference results in an offset to lateral force and pitching moment. A sudden drop in pitching moment (nose down) can be seen around $\Psi=110^{o}$ followed by a sharp increase (nose up) close to $\Psi=120^{o}$. This behaviour seems pretty much in line with the pressure fluctuation observed on the tail boom in Figure 12.d. The major part of pitch and roll moments is produced by the horizontal stabilizer. A 4/rev oscillation can be clearly observed indicating interference with the main rotor, as might be also anticipated by inspection of Figure 9. The position of the tail fin diminishes its contribution of to the overall roll moment owing to a short moment arm with respect to the rotor centre. Nevertheless, obvious aerodynamic interference with the tail rotor can be traced in the form of 10/rev fluctuations.

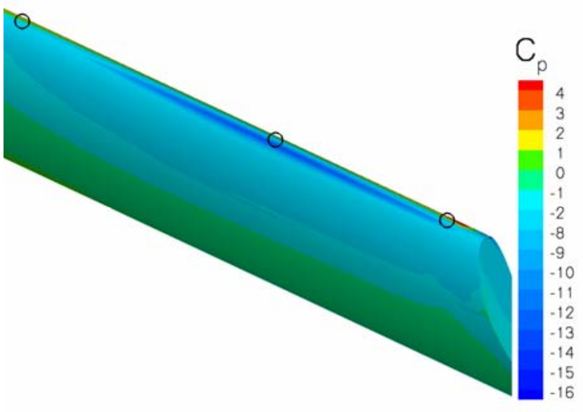

Figure 15: Pressure variation on the leading edge of the horizontal stabilizer in pitch up. Circles denote the location of pressure sensors.

Figure 17 presents the corresponding results for pitch up. Pitch up is associated with a reduction in the aerodynamic drag of the fuselage as the impingement of the rotor wake increases the force normal to the chord of the horizontal stabilizer. Due to the pitch angle considered, the normal force on the horizontal stabilizer becomes a forward (propulsive) force component which reduces the

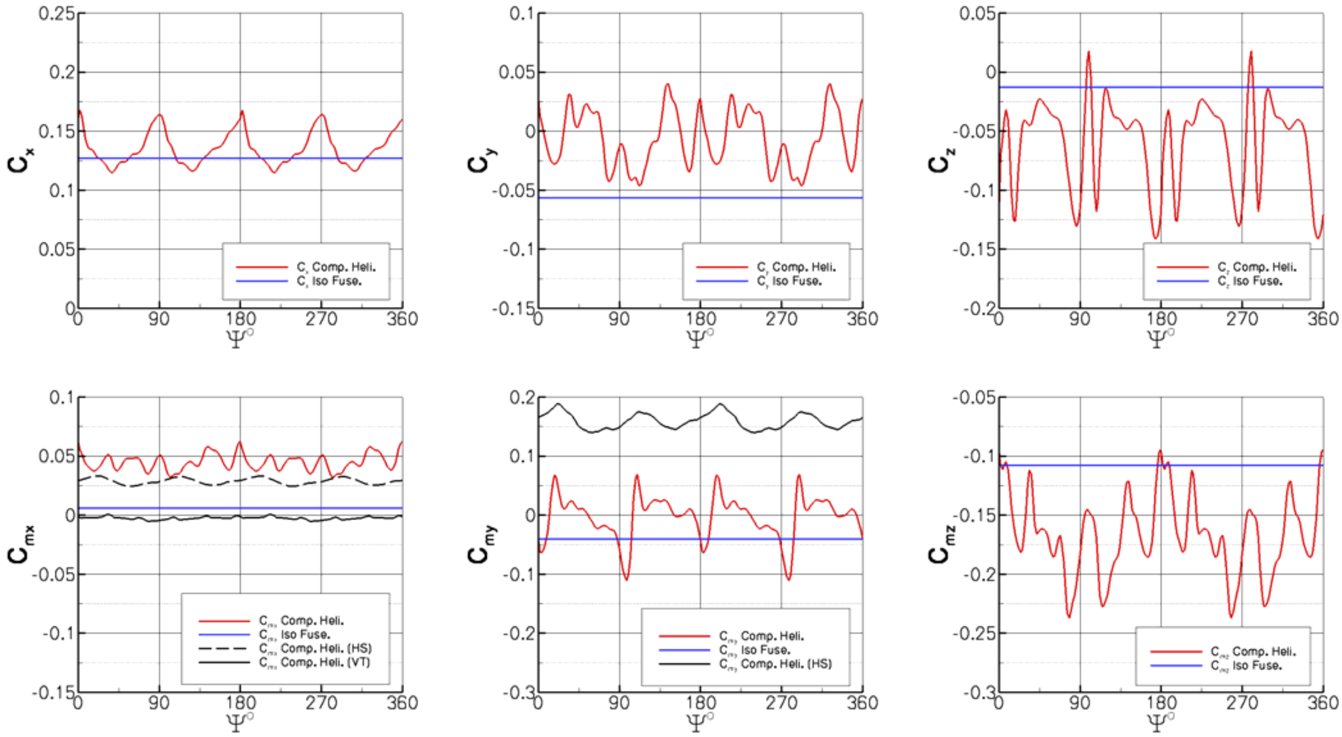

Figure 16: Comparison of computed fuselage forces for the complete helicopter case (red) and isolated fuselage (blue). Black curves correspond to the contribution of specific fuselage components. HS and VT respectively abbreviate horizontal stabilizer and vertical tail fin. Free stream mach number, Ma = 0.204, fuselage attitude, $\alpha = 2^{o}$.

overall drag of the fuselage by about 20% as shown in the figure. The drag of the isolated fuselage and the contribution of the horizontal stabilizer are shown for comparison. The evolution of the vertical force coefficient is characterized by strong 4/rev oscillations about a negative lift coefficient of -0.178. As far as the mean value is concerned, the major contribution is attributed to the horizontal stabilizer. Comparison with the isolated fuselage data reveals that the rotor downwash reverses the direction of lift generated on the stabilizer, as could also be predicted from Figure 14. A similarly dominant role of the stabilizer on roll moment can be observed. The influence of the tail rotor can be traced from the tail fin contribution to roll and yaw moment in the form of 10/rev pulsation. The figure demonstrates clearly development of pitch up. This can be deduced from the augmentation of the moment coefficient for the complete helicopter, which is mainly produced by negative lift acting on the stabilizer as mentioned earlier.

CONCLUSIONS

Results of steady and time-accurate RANS simulation of a complete helicopter configuration, its main rotor, and fuselage were presented. The main objective of the investigation was to analyse the aerodynamic interference between the rotating and non rotating elements of the aircraft. Weak fluid-structure coupling was iteratively applied to trim the main rotor to generate the same propulsive, lateral and vertical force in the isolated rotor and complete helicopter cases. Two flight conditions were considered where tail shake and pitch up would take place.

On the rotor blades, slight disagreement in the computed pressure was found between the isolated rotor and the complete helicopter. Noticeable differences between isolated rotor and complete helicopter could be observed for the normal load. A strong dependence of the normal load distribution on the rotor disc on the advance ratio was found. The aerodynamic interference resulted in different trim and blade dynamics expressed in phase shift and different peak values of rotor loads. However, all the observed differences had only a negligible impact on power consumption.

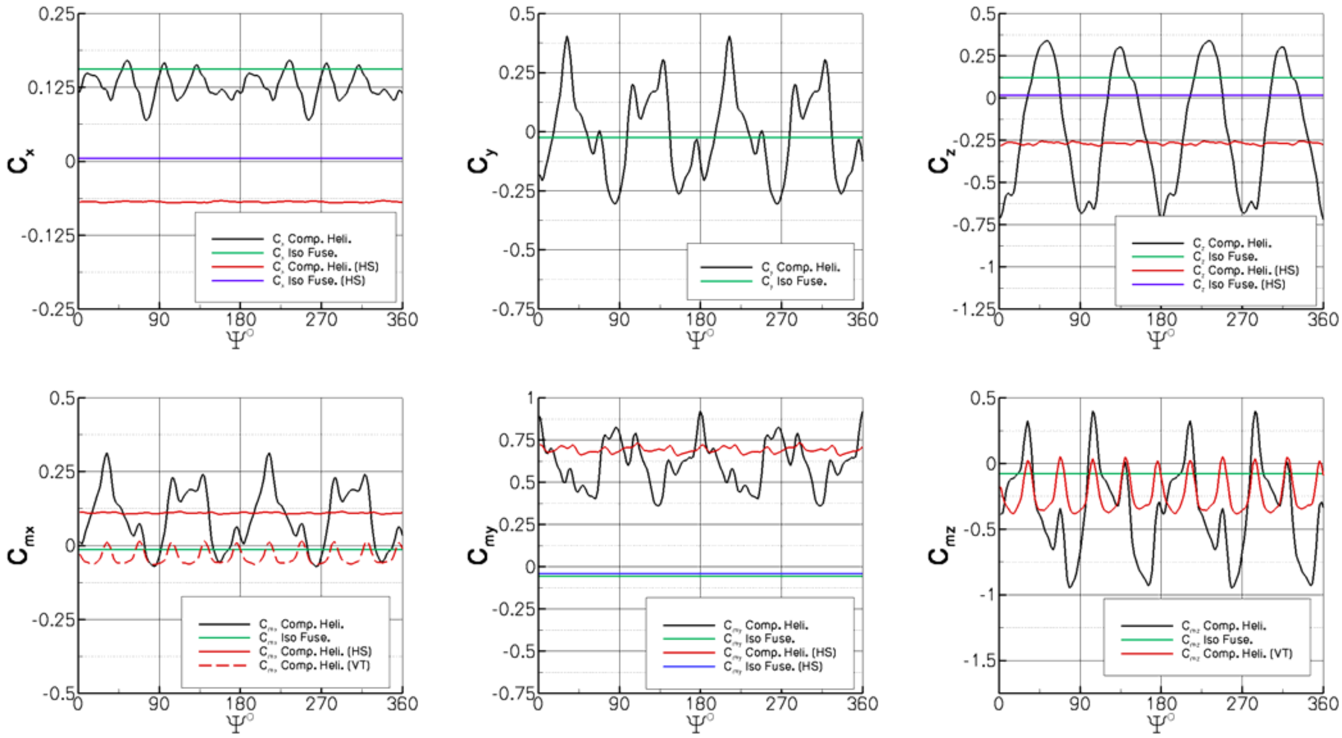

Figure 17: Comparison of computed fuselage forces for the complete helicopter case (black) and isolated fuselage (green) in pitch up. Red and blue curves, respectively, correspond to the contribution of specific fuselage components. HS and VT respectively abbreviate horizontal stabilizer and vertical tail fin. Free stream mach number, Ma = 0.059, fuselage attitude, $\alpha=5^{o}$.

Unlike the main rotor, the aerodynamic characteristics of the fuselage were strongly affected by the presence of the rotor. This could be demonstrated by analysing the computed surface pressure patterns and aerodynamic forces. Evolution of pitch up could be detected by several indicators, including an increase in pitching moment, surface pressure distribution and streamlines. The results indicated strong influence of the walls on the pressure inside the tunnel in the complete helicopter case. An analysis of the interference with the walls was not intended in this paper. However, it remains interesting to investigate the influence of the wall on the aerodynamic forces numerically, and to compare it with the empirical corrections applied in experiment.

The differences found between the isolated rotor and complete helicopter are too slight to be explained on physical grounds. There are numerous sources of uncertainty associated with the numerical simulation that must be assessed before a conclusive comment can be made. If these investigations revealed a similar outcome, may be then concluded with a certain degree of confidence that simulation of isolated rotors may be sufficient for the design and optimization of blades. However, it should be noted that the fuselage was placed in the wake of the rotor in the two flight conditions considered in the paper. Whether the rotor will remain insensitive to the presence of a fuselage under severer flight conditions, owing to physical reasons or otherwise, is unclear.

The study revealed considerable unsteady loading, which may be important in terms of frequency and/or strength to some design process. In this respect time-accurate computations are irreplaceable since actuator discs do neither provide information of the unsteady aerodynamic loads nor can be coupled with flight mechanics tools to trim the rotor. The question to which extent would such shortcomings influence the aerodynamics of the fuselage cannot be answered without a direct comparison of the presented data with actuator disc results.

ACKNOWLEDGEMENT

The major part of the computations reported in this paper was carried out within the European Union Specific Targeted Research Project GOAHEAD (GROWTH Contract Number AST4-CT-2005-516074). The authors would like to thank the European Union for financial support.

REFERENCES

[1] Freeman, C. E., Development and validation of a combined rotor-fuselage induced flow-field computational method. NASA TP 1656, 1980.

[2] Lorbee, P. E., Egolf, T. E., An unsteady helicopter rotor-fuselage aerodynamic interaction analysis. *Journal of the American Helicopter Society,* Vol. 35, No. 3, 1990. pp 32-42.

[3] Beaumier, P., Chelli, E., Pahlke, K., Navier-Stokes prediction of helicopter rotor performance in hover including aero-elastic effects, *56th Annual Forum of the American Helicopter Society, Virginia Beach, Virginia,* May 2000.

[4] Chelli, E., Pahlke, K., Calculation of Viscous flow around the BO105 main rotor in hover, DLR Internal Report IB-NR 129-99/27.

[5] Pahlke, K., Van der Wall, B., Calculation of multi-bladed rotors in high speed forward flight with weak fluid-structure coupling. *Proceedings of the 27th European Rotorcraft Forum, Moscow, Russia,* September 2001.

[6] Pomin, H., Wagner, S., Navier-Stokes analysis of helicopter rotor aerodynamics in hover and forward flight, AIAA Paper 2001-0998.

[7] Pomin, H., Wagner, S., Aeroelastic analysis of helicopter rotor blades on deformable Chimera grids, AIAA Paper 2002-0951.

[8] Khier, W., Navier-Stokes prediction of the effect of the skids on the aerodynamics of helicopter fuselage in forward flight, *Proceedings of the 32nd European Rotor Craft Forum, Maastricht, Holland*, September 2006.

[9] Khier, W., Schwarz, T., Application of Cartesian background grid in combination with Chimera method to predict aerodynamics of helicopter fuselage, *Proceedings of the 29th European Rotorcraft Forum, Friedrichshafen, Germany,* September 2003.

[10] D'Alascio, A., Berthe, A., Le Chuiton, F., Application of CFD to the fuselage aerodynamics of the EC145 helicopter. Prediction of unsteady phenomena and of the time averaged influence of the main rotor. *Proceedings of the 29th European Rotorcraft Forum, Friedrichshafen, Germany,* September 2003.

[11] D'Alascio, A., Pahlke, K., Le Chuiton, F., Application of a structured and an unstructured CFD-method to the fuselage aerodynamics of the EC145 helicopter. Prediction of the time averaged influence of the main rotor. *European Congress on Computational Methods in Applied Sciences and Engineering, ECCOMAS 2004, Jyväskylä,* July 2004.

[12] D'Alascio, A., Castellin, C., Schöning, B., Industrial validation of CFD solvers on medium and large helicopter fuselages. *Proceedings of the 31st European Rotorcraft Forum, Florence, Italy,* September 2005.

[13] Routhieau, V., Improved experimental and theoretical tools for helicopter aeromechanic and aeroacoustic interactions. Heliflow report Nr. HFLOW/4/EC/071. July 2001.

[14] Khier, W., Schwarz, T., Raddatz, J., Time-accurate simulation of the flow around the complete Bo105 wind tunnel model. *Proceedings of the 31st European Rotorcraft Forum, Florence, Italy,* September 2005.

[15] Khier, W., le Chuiton, F., Schwarz, T., Navier-Stokes analysis of the helicopter rotor-fuselage interference in forward flight, *CEAS Aerospace Aerodynamics Research Conference,* Cambridge, England, June 2002.

[16] Park, Y. M., Nam, H. J., Kwon, O. J., Simulation of unsteady rotor-fuselage interactions using unstructured adaptive meshes. *59th Annual Forum of the American Helicopter Society*, Phoenix, Arizona, May 2003.

[17] Brezillon, J., Simulation of rotor-fuselage interactions by using an actuator disc. *Proceedings of the 26th European Rotorcraft Forum*, The Hague, The Netherlands, September 2000.

[18] Renaud, T., O'Brien, D., Smith, M., Potsdam, M., Evaluation of isolated fuselage and rotor-fuselage interaction using CFD. *60th Annual Forum of the American Helicopter Society*, Baltimore, MD, June 2004.

[19] Dietz, M., Krämer, E., Wagner, S., Altmikus, A.: Weak coupling for active advanced rotors. *Proceedings of the 31st European Rotorcraft Forum, Florence, Italy,* September 2005.

[20] Dietz, M., Khier, W., Wagner, S., Numerical simulation of a full helicopter configuration using weak fluid-structure coupling. Accepted paper at 46th AIAA Aerospace Sciences Meeting and Exhibit, Reno, Nevada, January 2008.

[21] Dietz, M., Keßler, M., Krämer, E., Trimmed simulation of a complete helicopter configuration using fluid-structure coupling, to be published in high performance computing in science and engineering '07, Springer Verlag, 2007.a.

[22] Altmikus, A., Wagner, S., Beaumier, P., Servera, G., A comparison: weak versus strong modular coupling for trimmed aeroelastic rotor simulations. *58th Annual Forum of the American Helicopter Society,* Montreal, Canada, June 2002.

[23] Deutsches Zentrum für Luft- und Raumfahrt e.V. DLR, Generation of advanced helicopter experimental aerodynamic database for CFD code validation – GOAHEAD – Contract Nr. 516074: Annex I – Description of Work, November 2005.

[24] Pahlke, K., The GOAHEAD project, *Proceedings of the 33rd European Rotorcraft Forum, Kazan, Russia,* September 2007.

[25] Boelens, O.J., *et. al.*, The blind-test activity of the GOAHEAD project. *Proceedings of the 33rd European Rotorcraft Forum, Kazan, Russia,* September 2007.

[26] Kroll, N., Eisfeld, B., Bleecke, H.M., The Navier-Stokes Code FLOWer. *Volume 71 of Notes on Numerical Fluid Mechanics, pp. 58-71. Vieweg, Braunschweig,* 1999.

[27] Rudnik, R., Untersuchung der Leistungsfähigkeit von Zweigleichungs-Turbulenzmodellen bei Profilumströmungen, Deutsches Zentrum für Luft- und Raumfahrt e.V., FB 97-49.

[28] Wilcox, D. C., Reassessment of the scale-Determining equation for advanced turbulence models, AIAA Journal, vol. 26, no. 11, November 1988.

[29] Benek, J. A., Steger, J. L, Dougherty, F. C.: A Flexible grid embedding technique with application to the Euler equations, AIAA Paper 83-1944.

[30] Benoit, B., Dequin, A-M., Kampa, K., Grünhagen, W. v., Basset, P-M., Gimonet, B., HOST: A General Helicopter Simulation Tool for Germany and France. *56th Annual Forum of the American Helicopter Society, Virginia Beach, Virginia,* May 2000.